The identification of isoprenoids that bind in the intersubunit cavity of *Escherichia coli* 2C-methyl-D-erythritol-2,4-cyclodiphosphate synthase by complementary biophysical methods

Lauris E. Kemp,[a] Magnus S. Alphey,[a] Charles S. Bond,[a] Michael A. J. Ferguson,[a] Stefan Hecht,[b] Adelbert Bacher,[b] Wolfgang Eisenreich,[b] Felix Rohdich[b] and William N. Hunter[a]*

[a]Division of Biological Chemistry and Molecular Microbiology, School of Life Sciences, University of Dundee, Dundee DD1 5EH, Scotland, and [b]Institut für Organische Chemie und Biochemie, Technische Universität München, Lichtenbergstrasse 4, D-85747 Garching, Germany

Correspondence e-mail:
w.n.hunter@dundee.ac.uk

The discovery of a distinct metabolic pathway, the non-mevalonate or 1-deoxy-D-xylulose-5-phosphate (DOXP) pathway for isoprenoid precursor biosynthesis, in eubacteria and apicomplexan parasites has revealed a new set of potential drug targets. The emphasis of research on this pathway has been on delineating the intermediates and the biochemical and structural characterization of component enzymes. Two new monoclinic crystal forms of recombinant *Escherichia coli* 2C-methyl-D-erythritol-2,4-cyclodiphosphate (MECP) synthase cocrystallized with (i) CMP and (ii) CMP and MECP show well defined electron density at the subunit interface suggestive of an isoprenoid-like ligand. ^{31}P NMR analysis of the recombinant protein sample indicates the presence of bound diphosphate species and electrospray mass spectrometry identifies a mixture of isopentenyl diphosphate (and/or dimethylallyl diphosphate), geranyl diphosphate and farnesyl diphosphate in an approximate ratio of 1:4:2. The most prevalent species, geranyl diphosphate, was successfully modelled into the electron density, revealing the important protein–ligand interactions that stabilize binding of the isoprenoid. The observation that MECP synthase binds three metabolites that are produced by enzymes two, three and four stages downstream in isoprenoid biosynthesis suggests that feedback regulation of the non-mevalonate pathway is possible.

1. Introduction

Isoprenoids represent one of the largest groups of natural products and include numerous primary and secondary metabolites such as sterols, dolichols and triterpenes, components of cofactors and macromolecules such as the prenyl groups of chlorophyll, ubiquinones, prenylated proteins and isopentylated tRNAs (Rohmer, 1999; Sacchettini & Poulter, 1997). The structural diversity and chemical properties of isoprenoids are utilized in varied and important biological functions, including respiration, photosynthesis, transcriptional regulation and lipid-membrane biosynthesis (Goldstein & Brown, 1990).

Isopentenyl diphosphate (IPP) and dimethylallyl diphosphate (DMAPP) are the basic five-carbon building blocks for all isoprenoids and two biosynthetic pathways have evolved to supply these universal precursors. In mammals, fungi, a few species of bacteria and the cytosol of plants, IPP is synthesized through the well characterized mevalonate (MVA) pathway, which is named after one of the intermediates (Beytia & Porter, 1976; Boucher & Doolittle, 2000; Edwards & Ericsson, 1999; Goldstein & Brown, 1990). The MVA biosynthetic route involves seven enzymes and begins with the conversion of three molecules of acetyl-CoA to 3-hydroxy-3-methylglutaryl-

CoA. This is followed by a reduction, phosphorylation and decarboxylation to generate IPP, some of which is then isomerized to DMAPP.

The existence of a second mevalonate-independent pathway leading to IPP and DMAPP was discovered only recently (Rohmer et al., 1993; Schwarz, 1994). This pathway is called the non-mevalonate route, to distinguish it from the MVA pathway, or is alternatively named after two of the intermediates, the 1-deoxy-D-xylulose-5-phosphate (DOXP) or 2C-methyl-D-erythritol-4-phosphate (MEP) pathway (Eisenreich et al., 1998; Lichtenthaler, 1999; Rohmer, 1999). This pathway occurs in algae, the apicomplexa, chloroplasts, cyanobacteria and most eubacteria. The first stage in the DOXP pathway is the condensation of pyruvate and D-glyceraldehyde-3-phosphate to produce DOXP (Lois et al., 1998; Sprenger et al., 1997). The second and third stages of the pathway convert DOXP to MEP (Takahashi et al., 1998) and transfer the erythritol derivative onto a nucleotide, producing 4-diphosphocytidyl-2C-methyl-D-erythritol (CDP-ME; Rohdich et al., 1999). The ATP-dependent CDP-ME kinase then phosphorylates CDP-ME, forming 4-diphosphocytidyl-2C-methyl-D-erythritol-2-phosphate (CDP-ME2P) and ADP (Lüttgen et al., 2000). Next, CDP-ME2P is converted to 2C-methyl-D-erythritol-2,4-cyclodiphosphate (MECP) with the release of CMP in a reaction catalysed by MECP synthase, the subject of the present study (Fig. 1; Herz et al., 2000). The cyclodiphosphate, in two enzyme-catalysed stages, undergoes a reduction and elimination to 1-hydroxy-2-methyl-2-(E)-butenyl-4-diphosphate and then to IPP and DMAPP (Hecht et al., 2001; Rohdich et al., 2002).

The DOXP pathway is an essential aspect of metabolism in certain organisms, including some of the most serious human pathogens, and the constituent enzymes provide validated targets for broad-spectrum antimicrobial drug development (Bell et al., 2003; Jomaa et al., 1999). Research on the enzymes involved in the DOXP pathway has produced a good understanding of the structure–reactivity relationships in DOXP reductoisomerase (Reuter et al., 2002; Steinbacher et al., 2003; Yajima et al., 2002), MEP cytidylyltransferase (Kemp et al., 2003; Richard et al., 2001) and CDP-ME kinase from Escherichia coli (Miallau et al., 2003; Wada et al., 2003). With respect to MECP synthase, a series of crystal structures of the enzymes from E. coli, Haemophilus influenzae and Thermus thermophilus have revealed comprehensive details of the protein fold, substrate specificity and mechanism of catalysis (Kemp et al., 2002; Kishida et al., 2003; Lehmann et al., 2002; Richard et al., 2002; Steinbacher et al., 2002).

In the process of solving the highest resolution structures of E. coli MECP synthase (Kemp et al., 2002), including two new monoclinic crystal forms of the enzyme cocrystallized with (i) CMP and (ii) CMP with MECP (this work), we observed electron density indicative of a non-peptide ligand extending from the surface of the protein, near three arginine residues, down into a hydrophobic cavity formed at the trimer core. The chemical environment and shape of the electron density suggested that a diphosphate-lipid type of molecule might occupy this cavity. Richard et al. (2002) also commented on the

presence of extraneous density in their model determined at 2.8 Å resolution and indicated that a geranyl diphosphate (GPP) might be accommodated in the cavity. However, the Protein Data Bank (PDB) entries associated with that study do not include GPP. To complement and assist the crystallographic analyses we sought to identify the ligand or ligands, exploiting the power of electrospray mass spectrometry in combination with NMR.

2. Methods and materials

2.1. Preparation of MECP synthase and crystallization with MECDP and CMP

MECDP and the enzyme were obtained as described previously (Kemp et al., 2002; Steinbacher et al., 2002). The enzyme was incubated with (i) 2 mM $MnCl_2$ and 2 mM CMP or (ii) 2 mM $MnCl_2$, 2 mM CMP and 6 mM MECP for 2 h before crystallization by the hanging-drop vapour-diffusion method. Thin plates grew over 4 d to a maximum size of $0.05 \times 0.2 \times 0.4$ mm in drops assembled from 3 µl protein solution (at a concentration of 6 mg ml^{-1}) in 50 mM sodium chloride, 50 mM Tris–HCl pH 7.7 and 1 µl reservoir solution comprising 10–20% polyethylene glycol 2000, 0.1 M ammonium sulfate and 0.1 M sodium acetate pH 4.4–5.0.

2.2. Data collection and structure solution

Details are presented in Table 1. Crystals were maintained at 103 K in the presence of 2-methyl-2,4-pentanediol as a cryoprotectant and data were measured with a Quantum-4
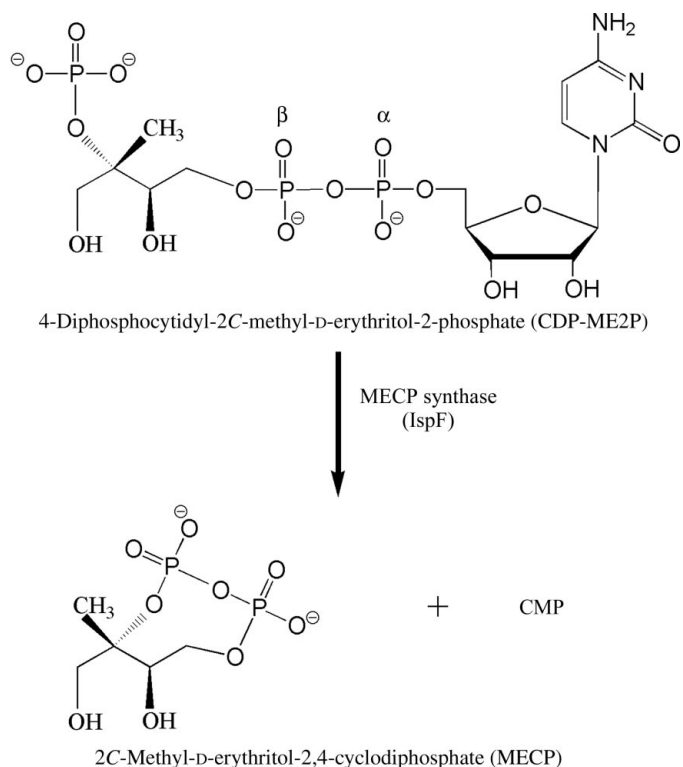

4-Diphosphocytidyl-2C-methyl-D-erythritol-2-phosphate (CDP-ME2P)

MECP synthase (IspF)

2C-Methyl-D-erythritol-2,4-cyclodiphosphate (MECP)   +   CMP

Figure 1
The reaction catalysed by MECP synthase, also known as IspF.

Table 1
Refinement and model-geometry statistics.

Values in parentheses are for the highest resolution shell.

Crystal form	I	II
Space group	$P2_1$	$C2$
Resolution (Å)	2.0	2.3
Wavelength (Å)	1.282	0.933
No. reflections	73529	73132
Completeness (%)	98.4 (95.9)	98.6 (86.3)
Redundancy	3.5	3.1
$I/\sigma(I)$	18.9 (3.0)	18.2 (1.6)
R_{sym}†	6.1	5.4
Wilson B factor (Å^2)	28.1	48.9
R_{work} (%)	21.4	19.5
R_{free} (%)	26.0	23.2
No. amino acids	943	946
No. protein atoms	7100	7159
No. water atoms	171	187
R.m.s. deviations‡		
Bond lengths (Å)	0.017	0.015
Angles (°)	1.62	1.55
Mean B factors (Å^2)		
Protein atoms	32.8	49.6
Solvent atoms	36.4	46.9
Zn^{2+}	63.3	55.7
CMP	40.1	93.5
MECP		65.8
GPP	52.3	76.5
Ramachandran analysis		
% in favoured regions	94.9	93.0
% in additionally allowed regions	5.1	7.0

† $R_{sym} = \sum |I - \langle I \rangle| / \sum I$, where I represents the measured intensity, $\langle I \rangle$ is the averaged intensity and the summation is over all symmetry-equivalent reflections. ‡ R.m.s. values are deviations from ideal values.

CCD detector (Area Detector Systems Corporation) on station ID14-EH4 at the European Synchrotron Radiation Facility (Grenoble, France). Data were processed and scaled with *DENZO/SCALEPACK* (Otwinowski & Minor, 1997).

Although grown under similar conditions and displaying the same morphology as the orthorhombic crystals studied previously, analysis of the diffraction data identified the presence of two new monoclinic crystal forms. Crystal form I, grown in the presence of MnCl$_2$ and CMP, displayed space group $P2_1$ with unit-cell parameters $a = 88.1$, $b = 117.5$, $c = 54.2$ Å, $\beta = 90.2°$. The unit-cell lengths are very similar to those of a previously characterized orthorhombic crystal form (PDB code 1gx1; Kemp *et al.*, 2002). Our first attempts at processing data from the new crystals were carried out assuming that we had obtained this orthorhombic form. However, despite using diffraction images of good quality, we noted a failure to predict the reflections correctly and very poor statistics. There were high χ^2 and R_{sym} values (13% overall), together with approximately 55 000 rejected measurements. This result suggested that the crystal was not orthorhombic. An alternative solution from autoindexing calculations was monoclinic with a β angle very close to 90°. Since we had measured 180° of data to record the anomalous dispersion signal from the Zn^{2+} ion bound in the active site, the change to lower symmetry did not compromise the data completeness. This monoclinic system proved satisfactory for data processing (for example, only 43 measurements were

rejected) and the subsequent analysis (Table 1). The data also provided a good anomalous signal to confirm the Zn^{2+} position (data not shown). Crystal form II, obtained in the presence of MnCl$_2$, CMP and MECP, exhibited space group $C2$ with unit-cell parameters $a = 198.1$, $b = 150.3$, $c = 57.6$ Å, $\beta = 106.5°$. Molecular replacement using the previously solved trimer as the search model (PDB code 1gx1; Kemp *et al.*, 2002) was carried out using *CNS* (Brünger *et al.*, 1998). The rotation searches were carried out using data within the resolution range 15–4 Å and produced a pair of three equivalent solutions for each crystal form, suggesting the presence of two trimers in the asymmetric unit. Translation searches then positioned the search model. The packing values calculated for the two trimers were 43 and 36% for forms I and II, respectively. These values are consistent with the estimated solvent content of 50% for form I and 65% for form II.

The *CCP*4 suite of programs was used for the analysis (Collaborative Computational Project, Number 4, 1994). Refinement was carried out with *REFMAC* (Murshudov *et al.*, 1997) combined with graphics inspection and model/map fitting with *O* (Jones *et al.*, 1991). A conservative approach to the identification of water molecules was adopted and a bulk-solvent scattering correction was applied. NCS (non-crystallographic symmetry) restraints were imposed in the early stages of the analyses and then released as the refinements progressed. The diphosphate groups are positioned on threefold NCS axes and GPP was modelled into this density. The lipid tails were refined with an occupancy of 0.33 in each of the threefold NCS positions. Molecular images were prepared with *PyMol* (DeLano, 2002) and *MOLSCRIPT* (Kraulis, 1991).
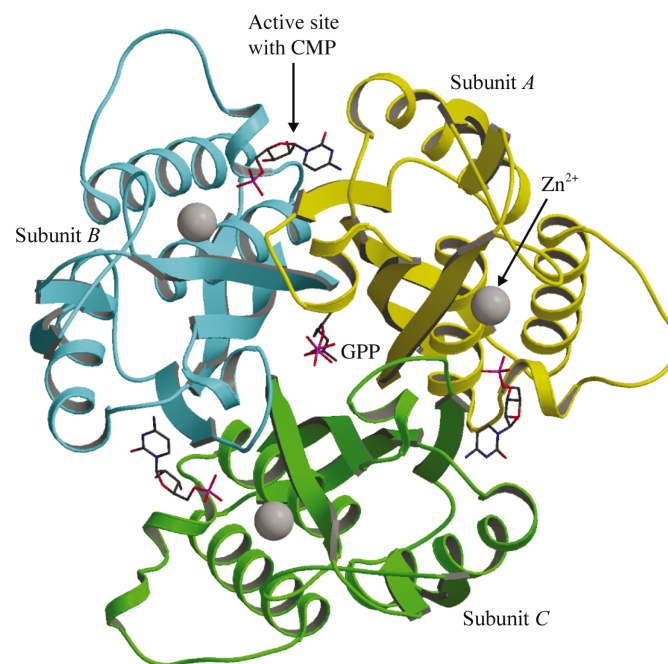

Figure 2
The functional MECP synthase trimer. Subunits are depicted as yellow, green and cyan ribbons. The Zn^{2+} ions (grey spheres) and CMP (stick representation) are shown in each active site. Geranyl diphosphate (GPP) is displayed in stick mode at the core of the trimer.

research papers

2.3. Mass spectrometry

4 µl aliquots of ice-cold ethanol were added to 20 µl of 28 mg ml^{-1} MECP until the solution was 80%(v/v) with respect to ethanol. This mixture was kept at 253 K overnight. Denatured and precipitated protein was removed by centrifugation (20 000g, 5 min, 277 K). The supernatant was adjusted to 5 mM with respect to ammonium acetate and introduced into the electrospray source of a Micromass Quattro Ultima triple-quadrupole mass spectrometer at 6 µl min^{-1}. Negative-ion spectra were collected. Standards of FPP and GPP (Sigma) were used to optimize ionization and collision conditions.

2.4. NMR spectroscopy

Samples for ^{31}P NMR measurements contained 100 mM Tris–HCl pH 8.0. The protein concentration was 2.5 mM. The samples contained 10%(v/v) ^{2}H$_2$O for the ^{2}H signal to lock the magnetic field. Precision NMR tubes (5 mm) were used for the acquisition of the spectra. The measurements were performed at 290 K on a Bruker DRX500 spectrometer operating at 202.5 MHz. Composite pulse ^{1}H decoupling was used. The spectra were recorded with a flip angle of 30° and a relaxation delay of 2.0 s. Quadrature detection and quadrature phase cycling were applied. The resulting free induction decays were processed by zero filling and exponential multiplication with a line-broadening factor of 2–20 Hz to improve the signal-to-noise ratio. 85% H$_3$PO$_4$ was used as an external reference.

3. Results

3.1. Overall structure

The MECP synthase subunit is a single α/β domain comprising 156 residues and consists of a four-stranded mixed β-sheet on one side with three α-helices on the other. Three subunits assemble into a compact bell-shaped trimer of approximately 45 × 56 Å in the axial and equatorial dimensions, respectively. This is the functional unit of the enzyme, as each active site is built from residues of two adjacent subunits; therefore, a trimer has three active sites between subunits A and B, B and C, and C and A (Fig. 2). Residues from pairs of subunits recognize and bind the substrate in an active site, which also contains a Zn^{2+} ion. This transition-metal ion was identified previously on the basis of anomalous dispersion measurements, X-ray absorption near-edge scans, atomic absorption spectroscopy and elemental analysis. The metal ion is bound to the enzyme by coordination with the side chains of Asp8, His10 and His42 (Kemp et al., 2002; Steinbacher et al., 2002). Either water or a phosphate O atom from a ligand completes the tetrahedral coordination geometry (not shown). The metal ion is probably acquired from the bacterial expression system. A second divalent cation can bind when substrate or CDP is in place to act in concert with the Zn^{2+} ion to align and polarize the substrate for catalysis to proceed (Kemp et al., 2002; Richard et al., 2002; Steinbacher et al., 2002). Under physiological conditions this is likely to be Mg^{2+}, although the addition of Mn^{2+} to the crystallization conditions

helped us to locate this ion-binding site near Glu135. At the core of the trimer is a large mainly hydrophobic cavity, which will be described later.

3.2. ^{31}P NMR

The ^{31}P NMR spectrum of the native wild-type MECP synthase from *E. coli* is shown in Fig. 3. The broad signals at −3.5 and −8.1 p.p.m. (linewidths 150 Hz) are assigned to the pyrophosphate moiety or moieties of the bound ligand(s). The narrower line (linewidth 7 Hz) observed at 3.6 p.p.m. appears to originate from inorganic phosphate. Indeed, the ^{31}P NMR spectrum displayed an increased signal at 3.6 p.p.m. after the addition of inorganic phosphate to the sample. As shown below, mass spectrometry of the protein extract indicates the presence of IPP, GPP and farnesyl diphosphate (FPP). Therefore, the detected broad ^{31}P NMR resonances of the protein might also reflect partial signal overlap of compounds resonating in the pyrophosphate region. Compared with free IPP (Rohdich et al., 2002), the pyrophosphate resonances are downfield shifted by 3–4 p.p.m. Since ^{31}P NMR chemical shifts are very sensitive towards differences in the O—P—O bond angles (Gorenstein, 1975), it can therefore be expected that small differences in the interaction between the pyrophosphate groups of the ligands and the apoprotein, which influence the dihedral angle of the O—P—O bond, lead to (relatively large) differences in the ^{31}P NMR spectra.

3.3. Identification of MECP synthase ligands by mass spectrometry

Negative-ion electrospray (ES) ionization and collision-induced dissociation (CID) conditions were optimized using GPP and FPP standards. These analyses showed that GPP and FPP produced intense phosphate, PO$_3^-$, and pyrophosphate, HP$_2$O$_6^-$, daughter ions at m/z 79 and 159 (Figs. 4a and 4b). A
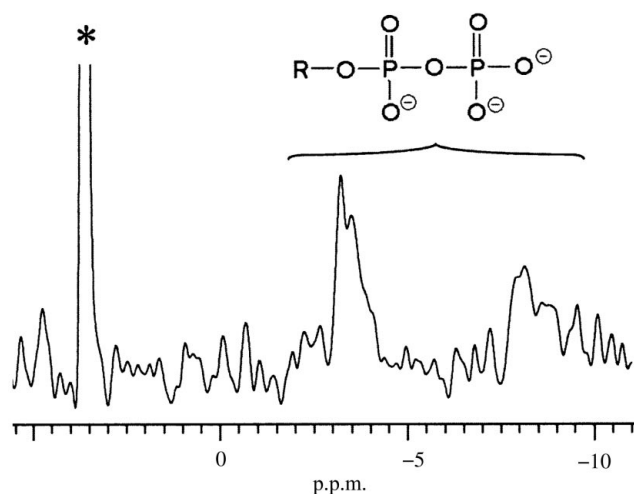
Figure 3
^{31}P NMR spectrum of MECP synthase. The truncated signal at 3.6 p.p.m. (indicated by *) is assigned as free phosphate present in the protein sample.

sample extracted from MECP synthase with 80%(v/v) ethanol was then analysed by ES–MS–CID–MS tandem mass-spectrometry scanning for parents of m/z 79 and m/z 159 (Figs. 4c and 4d). Three common parent ions were observed at m/z 245, 313 and 381, which correspond to those of IPP (and/or DMAPP), GPP and FPP. To confirm the identities of the latter two major species, daughter-ion spectra of these parent ions were recorded (Figs. 4e and 4f). These daughter-ion spectra are similar to those of the authentic GPP and FPP standards (Figs. 4a and 4b). Additional ions present in the sample daughter-ion spectra are likely to be because of the presence of unrelated molecular species in the crude sample that produce parent ions in the vicinity of m/z 313 and 381. The conclusion from this analysis is that IPP, GPP and FPP are bound to recombinant MECP synthase in an approximate ratio of 1:4:2. The sample used for crystallization contained this mixture of ligands, but we have not identified whether this ratio is carried over into the actual crystals themselves.

3.4. The hydrophobic cavity and isoprenoid binding

The quaternary structure of MECP synthase creates a triangular prism at the core of the homotrimer formed by the antiparallel alignment of three pairs of β1 and β6 strands, contributed by each of the monomers (Fig. 2). This core is approximately 16 Å distant from each of the three enzyme active sites.

The β-prism is fluted at the 'bottom' end (designated by the C-terminal end of strands β1, β4 and β5) forming an aperture (5 Å in diameter) that leads into a hydrophobic cavity, approximately 15 Å in length and 7.5 Å wide. The high-resolution crystal structure, determined in space group $P2_12_12$ at 1.8 Å resolution (Kemp et al., 2002), exhibited disjointed electron density within this hydrophobic cavity that could not be associated with any compounds present in the crystallization conditions. A sulfate (ammonium sulfate was used as a precipitant in crystallization) was modelled into the more defined density at the entrance to the cavity.

Fortuitously, the electron-density maps associated with the two new monoclinic crystal forms were more clearly defined and allowed us to model GPP in the cavity (shown for one form in Fig. 5) even though the resolutions of the analyses are slightly worse than those of the orthorhombic crystal form. The diphosphate moiety is positioned on the threefold NCS axis associated with the MECP synthase trimer. The diphosphate group was assigned full occupancy and the lipid tail an occupancy of 0.33 in each of the three positions around the NCS axis, one of which is shown in Fig. 5 together with the important side chains that form the core of the trimer.
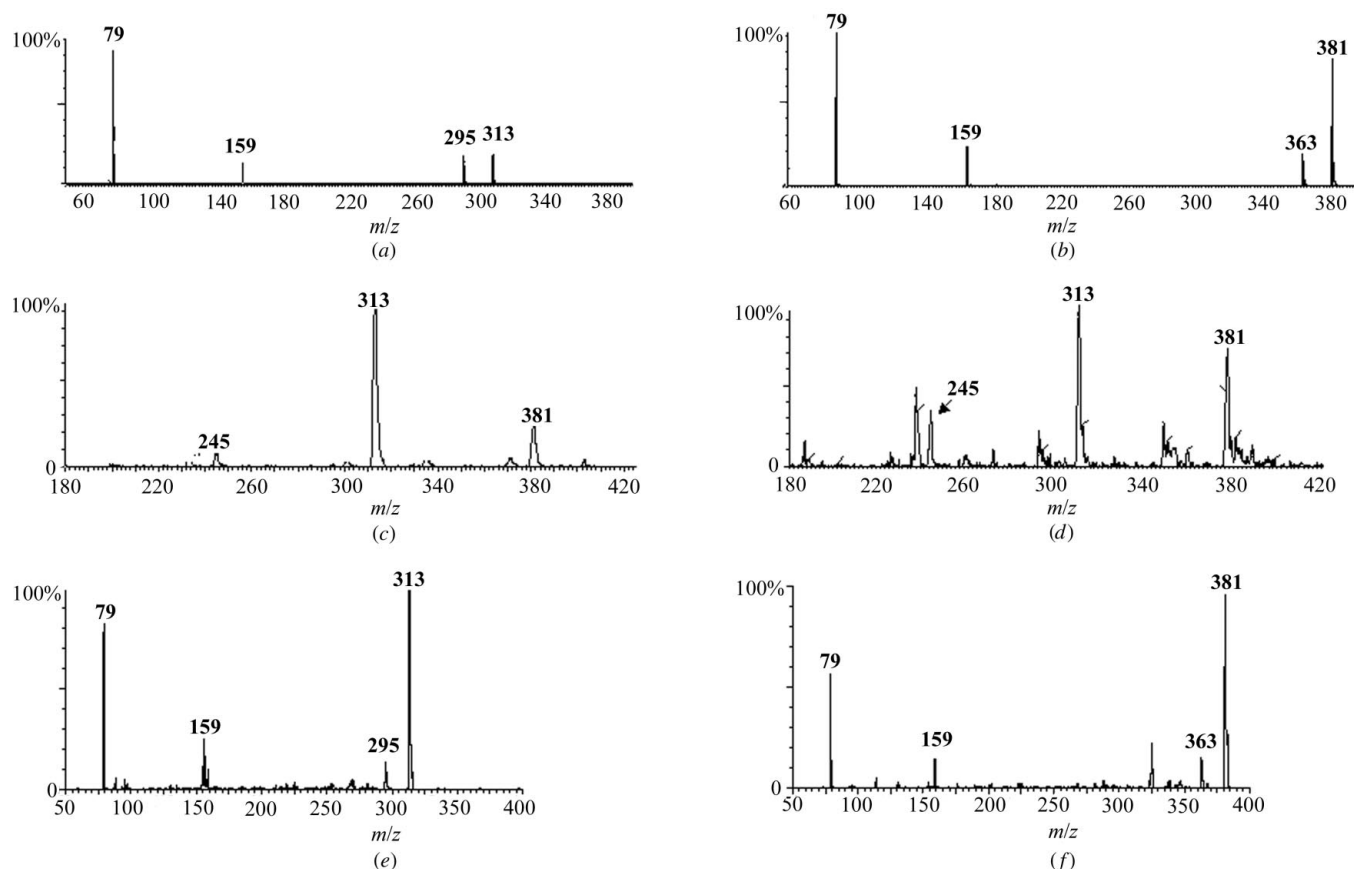

Figure 4
Negative-ion electrospray mass spectra of the extract from MECP synthase. (a) Daughter-ion scan of geranyl standard. (b) Daughter-ion scan of farnesyl diphosphate standard. (c) Sample parent-ion scan of m/z = 79 ion (PO_3^-). (d) Sample parent-ion scan of m/z = 159 ion ($HP_2O_6^-$). (e) Sample daughter-ion scan of m/z = 313 ion. (f) Sample daughter-ion scan of m/z = 381 ion.

Three δ-guanidino side chains, contributed by Arg142 from each monomer, position the outermost solvent-exposed phosphoryl O atoms of GPP (Fig. 6). These arginines are in turn held in place by salt-bridge interactions with three glutamic acids (Glu144). These residues guard the entrance to the hydrophobic core of the trimer and are highly conserved in other sequences of MECP synthase, suggesting that this phosphate-binding site is an important feature of the enzyme. In 43 of the 58 sequences currently available for MECP synthase, the Arg142–Glu144 (*E. coli* numbering) salt-bridge combination is strictly conserved. In a further nine sequences the acid/base combination is preserved although the identity of one of the partners is different. For example, in *Plasmodium falciparum* MECP synthase Glu142 replaces Arg142 and Lys144 replaces Glu144. A similar switching of residues is also seen in *Arabidopsis thaliana*, *Catharanthus roseus* and *Synechococcus* sp.

The second phosphate group of GPP accepts hydrogen bonds from the main-chain amide groups of Phe139 (not shown). The GPP tail then drops into a hydrophobic cavity lined with six phenylalanines (three Phe7 and Phe139 combinations), three valines and three isoleucines (Val9 and Ile99) and the aliphatic side chains of Thr134, Thr140 and Ala147, again from each monomer (Fig. 6). The GPP tail makes van der Waals contacts with Phe7 and Phe139 in particular. Three acidic residues, Glu149 from each subunit, lie close together and seal the other end of the cavity. Their proximity suggests that protonation has occurred and they are also held in place by hydrogen-bonding interactions with histidines (His5).

The NMR and mass-spectrometry data indicate that MECP synthase binds phosphate, IPP or DMAPP, GPP and FPP, the most abundant of the isoprenoid ligands being GPP. We were able to successfully model and refine GPP bound to the hydrophobic cavity of the enzyme. For simplicity, we refined the lipid tail at an occupancy of 0.33 in each of the three orientations observed in each hydrophobic cleft. Given that our best diffraction data were still only at a resolution of 2.0 Å, we did not see any benefit to employing alternative models in the refinement by including IPP or FPP in addition to GPP. The hydrophobic cavity would easily accommodate IPP as a ligand, but we note that in order to bind FPP some alteration of side-chain conformation at the base of the hydrophobic cleft would be required.

The two new monoclinic structures are very similar to each other and also to the orthorhombic structure reported previously. For example, a least-squares superposition of one trimer from crystal form I with the trimer of the orthorhombic form (PDB code 1gx1) produces an r.m.s. deviation of 0.31 Å for 471 C^α atoms. This close similarity extends also to side-chain groups and in particular to those residues that comprise the hydrophobic core and that interact with GPP (Fig. 7). We cannot rule out the possibility of a conformational change occurring upon binding an isoprenoid ligand at the core of the trimer because we do not yet have any structure of the *E. coli* enzyme proven to represent the apo form.

The entrance to the hydrophobic cavity would probably represent a major phosphate-binding site, although given that the catalytic centre has to process a substrate carrying three phosphate groups it is
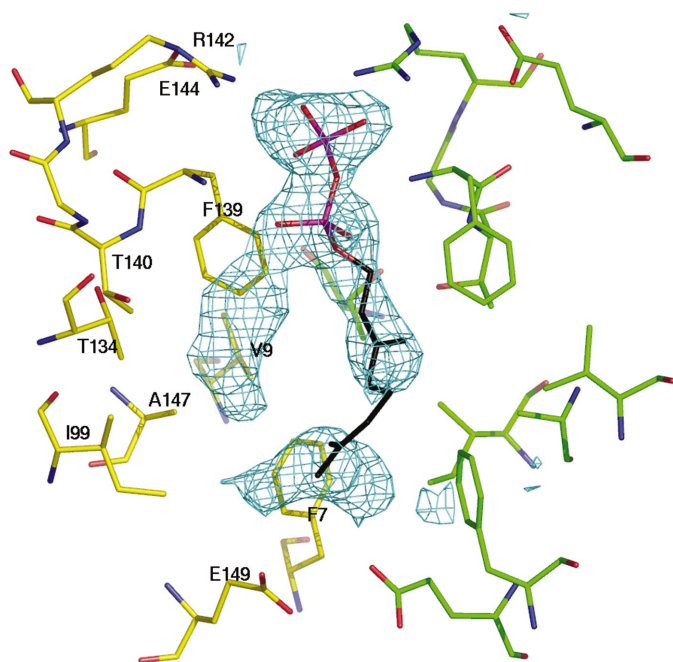

Figure 5
The omit $|F_o - F_c|\alpha_c$ difference density map (blue chicken wire) observed at one trimer interface in the $P2_1$ crystal form. The map is contoured at the 2.5σ level. Residues corresponding to the refined model from only two subunits are shown, with C positions coloured yellow and green for subunits *A* and *C*, respectively. N, P and O positions are coloured blue, purple and red, respectively, and the GPP C tail is black.
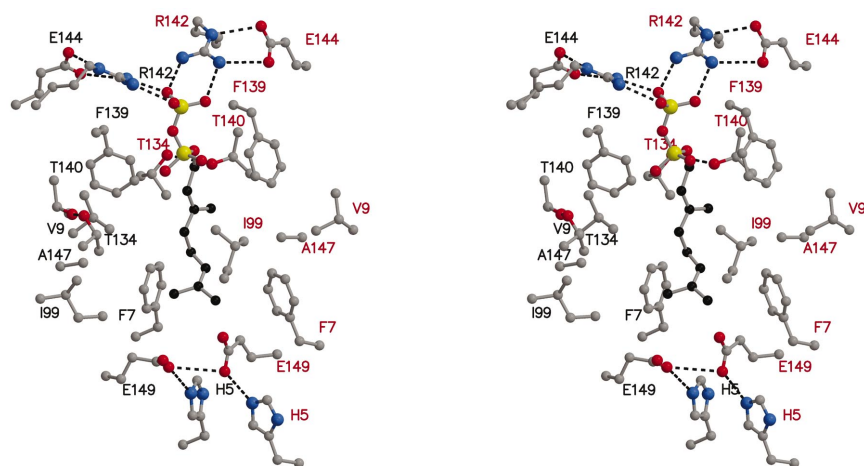

Figure 6
The GPP-binding site. For clarity, only side chains from subunit *A* (black labels) and *C* (red labels) are shown in ball-and-stick mode, coloured grey for C, blue for N and red for O atoms. The GPP atoms are coloured yellow for P, black for C and red for O atoms. Hydrogen-bonding interactions are depicted as dashed lines.

possible that the oxyanion can also bind in the active site, and there are also a number of basic residues on the surface of the enzyme that might interact with oxyanions.

3.5. Binding of CMP and MECP

Previous studies have determined the structures of MECP synthase with a number of ligands, including CMP and the substrate MECP in the active site. We were able to determine the structures of complexes with CMP and MECP in two new crystal forms, which diffracted to a slightly improved resolution compared with previous studies. Our analyses serve to confirm the previous work and the structures are so similar that we only make a few general comments. The importance of the new crystal forms is that they have provided electron density to clearly identify isoprenoid binding in the hydrophobic cavity at the core of the trimer.

Previously, it was shown that the cytosine moiety is bound to an aliphatic pocket consisting of conserved residues from one subunit. The ribose hydroxyl groups form direct hydrogen-bonding interactions with the carboxylate group of Asp56 and the amide group of Gly58. An Mn^{2+} or Mg^{2+} ion bridges the α- and β-phosphates and additionally coordinates Glu135 from another subunit and three solvent atoms.
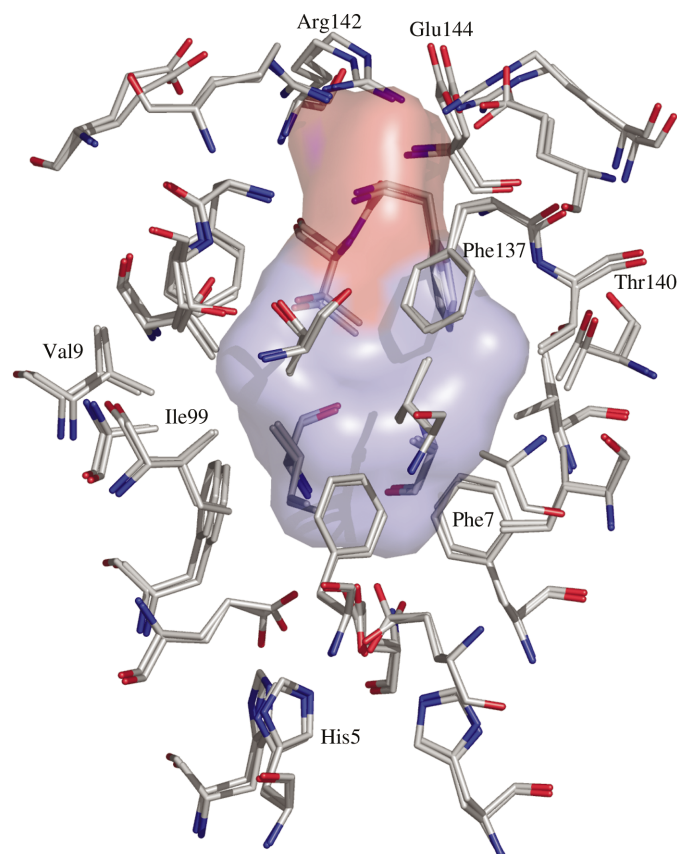

Figure 7
Overlay of two structures in the region of the hydrophobic cleft: the original 1.8 Å resolution orthorhombic form and the $P2_1$ crystal form. GPP is depicted as a semi-transparent surface coloured red for O and slate blue for C atoms. The protein residues are shown in stick mode, coloured grey for C, blue for N and red for O atoms. Selected amino acids are labelled.

Another metal ion, Zn^{2+}, is held tightly in place by residues of the adjacent subunit (His10, His42 and Asp8) and tethers the β-phosphate to one side of the active site.

In the $MnCl_2$ and CMP complex, the Zn^{2+} ion and CMP group are in the same positions as the Zn^{2+} ion and CDP group in the aforementioned structure (Kemp *et al.*, 2002). A solvent atom is found in place of the β-phosphate. The Mn^{2+} ion is absent, suggesting a requirement for two phosphate groups in the active site to create the right environment to bind a divalent cation in that position. It is likely that this cation, necessary for catalysis, will be recruited either with the substrate or following the binding of the substrate in the active site.

MECP synthase was cocrystallized with CMP and MECP. The highly conserved His34 and the loop comprising residues Pro62 through to Lys69, which are disordered in the absence of the product, are clearly defined when the product occupies the active site (Richard *et al.*, 2002; Steinbacher *et al.*, 2002). Despite a concentration of 6 m*M* MECP (compared with an enzyme concentration of approximately 0.15 m*M*), there is only difference density (approximately 8σ, where σ is the standard deviation of the electron density; data not shown) at the position of the phosphate ions using the MECP synthase structures solved at lower resolution as a guide. The rest of the product is less well defined by the electron density. It is possible that some degradation of MECP has occurred and that a mixture of compounds, the intact cyclodiphosphate and its breakdown products, occupy the active site. Previous *E. coli* MECP synthase structures at 2.5 and 2.8 Å have shown density for the diphosphate cyclic product with overall *B* factors of approximately 47 and 90 Å^2, respectively. The 2.5 Å structure was the result of soaking the crystal with 2 m*M* MECP for 1 h (Kemp *et al.*, 2002), whereas cocrystallization with 5 m*M* CMP, 5 m*M* MECP and 10 m*M* $MgCl_2$ produced the 2.8 Å structure (Richard *et al.*, 2002). In addition, the pH values at which our crystals and those for the ordered MECP structures were grown were not significantly different.

4. Discussion

The regulation of metabolic pathways often involves a mechanism dependent on the levels of one or more products of reactions catalysed by the component enzymes. Examples of this type of feedback regulation include isoprenoid-precursor biosynthesis by the MVA pathway (Goldstein & Brown, 1990) and amino-acid (Umbarger, 1978) and purine-nucleotide biosynthesis (Wyngaarden, 1976). The production of IPP in the DOXP pathway involves two enzymes that follow after MECP synthase: IspG and IspH (Hecht *et al.*, 2001; Rohdich *et al.*, 2002). Some IPP is converted to DMAPP by IPP isomerase; GPP synthase then utilizes the pool of IPP and DMAPP to produce GPP (Kellogg & Poulter, 1997). Next, the enzyme FPP synthase catalyses a reaction between GPP and IPP to generate FPP (Leyes *et al.*, 1999).

The critical observation we report is that mass spectrometry clearly identifies IPP (and or the isomer DMAPP), GPP and FPP binding to a purified recombinant MECP synthase and

that NMR confirms the presence of diphosphate. Crystallographic studies, greatly assisted by this knowledge, have provided structural details of the interactions of GPP with the enzyme. The fortuitous observation of isoprenoids binding to MECP synthase may just be coincidence. However, we note that these ligands are synthesized in steps catalysed by two, three or four enzymes downstream of MECP synthase and that the structural analysis of the GPP complex shows interactions with well conserved residues in a hydrophobic core created by the quaternary structure of the enzyme. The possibility exists that there may be feedback regulation of isoprenoid biosynthesis with MECP synthase as a point of control. Further experiments will be required to substantiate such a hypothesis, but it is worthy of note that should it be proven that MECP synthase is a regulatory checkpoint for isoprenoid biosynthesis then the value of this particular enzyme as a target for the development of new antimicrobial agents would be significantly enhanced.

References

Bell, B., Ruangweerayut, R., Wiesner, J., Missinou, M. A., Shindler, A., Baranek, T. & Hintz, M. (2003). *Antimicrob. Agents Chemother.* **47**, 735–738.

Beytia, E. D. & Porter, J. W. (1976). *Annu. Rev. Biochem.* **45**, 113–142.

Boucher, Y. & Doolittle, W. F. (2000). *Mol. Microbiol.* **37**, 703–716.

Brünger, A. T., Adams, P. D., Clore, G. M., Delano, W. L., Gros, P., Grosse-Kunstleve, R. W., Jiang, J.-S., Kuszewski, K., Nilges, M., Pannu, N. S., Read, R. J., Rice, L. M., Simonson, T. & Warren, G. L. (1998). *Acta Cryst.* D**54**, 905–921.

Collaborative Computational Project, Number 4 (1994). *Acta Cryst.* D**50**, 760–763.

DeLano, W. L. (2002). *PyMol.* http://www.pymol.org.

Edwards, P. A. & Ericsson, J. (1999). *Annu. Rev. Biochem.* **68**, 157–185.

Eisenreich, W., Schwarz, M., Cartayrade, A., Arigoni, D., Zenk, M. H. & Bacher, A. (1998). *Chem. Biol.* **5**, R221–R233.

Goldstein, J. L. & Brown, M. S. (1990). *Nature (London)*, **343**, 425–428.

Gorenstein, D. G. (1975). *J. Am. Chem. Soc.* **97**, 898–900.

Hecht, S., Eisenreich, W., Adam, P., Amslinger, S., Kis, K., Bacher, A., Arigoni, D. & Rohdich, F. (2001). *Proc. Natl Acad. Sci. USA*, **98**, 14837–14842.

Herz, S., Wungsintaweekul, J., Schuhr, C. A., Hecht, S., Lüttgen, H., Sagner, S., Fellermeier, M., Eisenreich, W., Zenk, M. H., Bacher, A. & Rohdich, F. (2000). *Proc. Natl Acad. Sci. USA*, **97**, 2486–2490.

Jomaa, H., Wiesner, J., Sanderbrand, S., Altincicek, B., Weidemeyer, C., Hintz, M., Turbachova, I., Eberl, M., Zeidler, J., Lichtenthaler, H. K., Soldati, D. & Beck, E. (1999). *Science*, **285**, 1573–1576.

Jones, T. A., Zou, J. Y., Cowan, S. W. & Kjeldgaard, M. (1991). *Acta Cryst.* A**47**, 110–119.

Kellogg, B. A. & Poulter, C. D. (1997). *Curr. Opin. Chem. Biol.* **1**, 570–578.

Kemp, L. E., Bond, C. S. & Hunter, W. N. (2002). *Proc. Natl Acad. Sci. USA*, **99**, 6591–6596.

Kemp, L. E., Bond, C. S. & Hunter, W. N. (2003). *Acta Cryst.* D**59**, 607–610.

Kishida, H., Wada, T., Unzai, S., Kuzuyama, T., Takagi, M., Terada, T., Shirouzu, M., Yokoyama, S., Tame, J. R. H. & Park, S. Y. (2003). *Acta Cryst.* D**59**, 23–31.

Kraulis, P. J. (1991). *J. Appl. Cryst.* **24**, 946–950.

Lehmann, C., Lim, K., Toedt, J., Krajewski, W., Howard, A., Eisenstein, E. & Herzberg, O. (2002). *Proteins*, **49**, 135–138.

Leyes, A. E., Baker, J. A. & Poulter, C. D. (1999). *Org. Lett.* **7**, 1071–1073.

Lichtenthaler, H. K. (1999). *Annu. Rev. Plant Physiol. Plant Mol. Biol.* **50**, 47–65.

Lois, L. M., Campos, N., Putra, S. R., Danielsen, K., Rohmer, M. & Boronat, A. (1998). *Proc. Natl Acad. Sci. USA*, **95**, 2105–2110.

Lüttgen, H., Rohdich, F., Herz, S., Wungsintaweekul, J., Hecht, S., Schuhr, C. A., Fellermeier, M., Sagner, S., Zenk, M. H., Bacher, A. & Eisenreich, W. (2000). *Proc. Natl Acad. Sci. USA*, **97**, 1062–1067.

Miallau, L., Alphey, M. S., Kemp, L. E., Leonard, G. A., McSweeney, S. M., Hecht, S., Bacher, A., Eisenreich, W., Rohdich, F. & Hunter, W. N. (2003). *Proc. Natl Acad. Sci. USA*, **100**, 9173–9178.

Murshudov, G. N., Vagin, A. A. & Dodson, E. J. (1997). *Acta Cryst.* D**53**, 240–255.

Otwinowski, Z. & Minor, W. (1997). *Methods Enzymol.* **276**, 307–326.

Reuter, K., Sanderbrand, S., Jomaa, H., Wiesner, J., Steinbrecher, I., Beck, E., Hintz, M., Klebe, G. & Stubbs, M. T. (2002). *J. Biol. Chem.* **277**, 5378–5384.

Richard, S. B., Bowman, M. E., Kwiatkowski, W., Kang, I., Chow, C., Lillo, A. M., Cane, D. E. & Noel, J. P. (2001). *Nature Struct. Biol.* **8**, 641–648.

Richard, S. B., Ferrer, J. L., Bowman, M. E., Lillo, A. M., Tetzlaff, C. N., Cane, D. E. & Noel, J. P. (2002). *J. Biol. Chem.* **277**, 8667–8672.

Rohdich, F., Hecht, S., Gärtner, K., Adam, P., Krieger, C., Amslinger, S., Arigoni, D., Bacher, A. & Eisenreich, W. (2002). *Proc. Natl Acad. Sci. USA*, **99**, 1158–1163.

Rohdich, F., Wungsintaweekul, J., Fellermeier, M., Sagner, S., Herz, S., Kis, K., Eisenreich, W., Bacher, A. & Zenk, M. N. (1999). *Proc. Natl Acad. Sci. USA*, **96**, 11758–11763.

Rohmer, M. (1999). *Comprehensive Natural Products Chemistry: Isoprenoids Including Carotenoids and Steroids*, edited by D. Barton & K. Nakanishi, Vol. 2, pp. 45–67. Amsterdam: Elsevier.

Rohmer, M., Knani, M., Simonin, P., Sutter, B. & Sahm, H. (1993). *Biochem. J.* **295**, 517–524.

Sacchettini, J. C. & Poulter, C. D. (1997). *Science*, **277**, 1788–1789.

Schwarz, M. K. (1994). PhD thesis No. 10978, ETH Zürich, Switzerland.

Sprenger, G. A., Schorken, U., Weigert, T., Grolle, S., de Graaf, A. A., Taylor, S. V., Begley, T. P., Bringer-Meyer, S. & Sahm, H. (1997). *Proc. Natl Acad. Sci. USA*, **94**, 12857–12862.

Steinbacher, S., Kaiser, J., Eisenreich, W., Huber, R., Bacher, A. & Rohdich, F. (2003). *J. Biol. Chem.* **278**, 18401–18407.

Steinbacher, S., Kaiser, J., Wungsintaweekul, J., Hecht, S., Eisenreich, W., Gerhardt, S., Bacher, A. & Rohdich, F. (2002). *J. Mol. Biol.* **316**, 79–88.

Takahashi, S., Kuzuyama, T., Watanabe, H. & Seto, H. (1998). *Proc. Natl Acad. Sci. USA*, **95**, 9879–9884.

Umbarger, H. E. (1978). *Annu. Rev. Biochem.* **47**, 533–606.

Wada, T., Kuzuyama, T., Satoh, S., Kuramitsu, S., Yokoyama, S., Unzai, S., Tame, J. R. & Park, S. Y. (2003). *J. Biol. Chem.* **278**, 30022–30027.

Wyngaarden, J. B. (1976). *Adv. Enzyme Regul.* **14**, 25–42.

Yajima, S., Nonaka, T., Kuzuyama, T., Seto, H. & Ohsawa, K. (2002). *J. Biochem. (Tokyo)*, **131**, 313–317.